

Received 17 November 2023, accepted 27 November 2023, date of publication 30 November 2023,  
date of current version 6 December 2023.

Digital Object Identifier 10.1109/ACCESS.2023.3338222

## RESEARCH ARTICLE

# Carrier Harmonic Modulation for Simultaneous Wireless Information and Power Transfer

JAEMYUNG LIM<sup>1</sup>, (Member, IEEE), AND BYUNGHUN LEE<sup>1,2</sup>, (Member, IEEE)

<sup>1</sup>Department of Electronic Engineering, Hanyang University, Seoul 04763, South Korea

<sup>2</sup>Department of Biomedical Engineering, Hanyang University, Seoul 04763, South Korea

Corresponding author: Byunghun Lee (blee22@hanyang.ac.kr)

This work was supported in part by the Technology Innovation Program (Development of Low-Power Sensors and Self-Charging Power Sources for Self-Sustainable Wireless Sensor Platforms) funded by the Ministry of Trade, Industry and Energy (MI, South Korea) under Grant RS-2022-00154983; and in part by the National Research Foundation of Korea (NRF) Grant funded by the Korean Government under Grant 2021R1C1C1009986.

**ABSTRACT** This paper presents the carrier harmonic modulation (CHM) for near-field data communication during wireless power transmission. The proposed CHM does not increase the coil dimension, and an additional data driver is not required. Compare to conventional modulation techniques such as frequency-shift keying (FSK) and amplitude-shift keying (ASK), the power delivered to the load (PDL) of CHM is independent of the data transmission. The prototype CHM provides a data rate of 1.1 Mbps while the power carrier frequency is also 1.1 MHz. It achieved a maximum PDL of 641 mW and the system efficiency of 17% with a 30 mm TX/RX coil diameter.

**INDEX TERMS** Inductive link, downlink, data telemetry, wireless power transfer, SWIPT.

## I. INTRODUCTION

Wireless power transmission (WPT) has been widely adopted in a variety of applications from charging electric vehicles to internet-of-things (IoT) [1]. Because the supply connection wire, which would be the thickest in the system, is removed, it is also desired to eliminate the wired data line to make the system fully wireless. Therefore, simultaneous wireless information and power transfer (SWIPT) has been studied which delivers both power and data in the near-field WPT condition.

Conventional SWIPTs transfer data with an independent data communication channel [2] or the same WPT inductive link [3], [4]. If a system requires a high data rate, the former is preferable because the data rate of the latter is limited by the power carrier. However, the former requires an additional high-frequency oscillator followed by a data link driver for the extra link (antenna or coil), and it costs a significant amount of area and power [5]. If the data rate is far less than the power carrier frequency, the latter which modulates the power carrier with data is preferred. In general, three modulation techniques are widely used for power

carrier modulation: Amplitude-shift keying (ASK), phase-shift keying (PSK), and frequency-shift keying (FSK). ASK changes the power delivered to the load (PDL) which is proportional to the amplitude of the carrier. On the other hand, PSK causes a portion of power reflected at the transmitter (TX) while changing the phase [4] resulting in lower PDL. FSK modulates the carrier frequency based on the data, and it is impossible to achieve the maximum PDL on both data bits (0 and 1), especially on the high-quality (Q)-factor coil [6].

There have been studies about utilizing the harmonics in data telemetry to improve data rate. In [7], the RX generates a harmonic frequency from the power carrier, and it is used as a data carrier of uplink by using on-off keying modulation. However, it does not provide downlink communication. A pulse harmonic modulation (PHM) [8] utilizes an impulse to transfer a data stream and another impulse to cancel the harmonic oscillation and reduce inter-symbol interference (ISI). However, PHM is a data telemetry technique that requires additional data links. In addition, it is extremely sensitive to the delay and amplitude variation of the impulses. A pulse delay modulation (PDM) in [9] applies an impulse at the zero-crossing point of the power carrier, and the RX extracts data by measuring the delay of the zero crossing points. The

The associate editor coordinating the review of this manuscript and approving it for publication was Diego Masotti<sup>1</sup>.

PDM also requires precise control of the impulse timing to apply at the exact zero crossing point, and it requires complex calibration for a specific wireless link condition [10]. In the previous study mentioned in [11], FSK was used, and the data was detected in the harmonic frequency to amplify the frequency difference. However, since this method still uses FSK, it is not possible to maximize PDL. The study in [12] employs the 3<sup>rd</sup> harmonic generated as a byproduct of the rectifier, but the technique requires an additional antenna that is completely separated from the WPT coil and is not applicable for the downlink.

In this work, we proposed the new concept of carrier harmonic modulation (CHM) based on near-field WPT which provides a high data rate (equal to the carrier frequency) without an additional high-frequency oscillator, driver, and strict timing requirement. In the CHM, for both receiver (RX) and TX, three coils (one square-shaped and two 8-shaped coils) that overlap each other (Fig. 1) are used, however, they are connected and worked as a merged coil. As the three coils are placed on the same layer, the utilization of three coils does not result in an increase in dimension. Furthermore, a high data rate SWIPT system employing multiple coils, such as the LCCL topology [13], necessitates an additional transformer that blends high-frequency data with the power carrier. Nevertheless, its size renders it impractical for implementation in biomedical applications.

In TX, the three coils are connected in parallel, and a single power amplifier (PA) drives all of them at the same time. In RX, the three coils are connected. The fundamental frequency of the main carrier is utilized as a main power delivery carrier, and the two harmonics which are derived from the carrier are used as 2-bit simultaneous data transmission. Moreover, as the data communication is entirely isolated from the power link, we can optimize the PDL regardless of data transmission.

In section II, the concept of the proposed CHM is introduced. The simulation and measurement results for a proof-of-concept CHM are verified and compared in section III, followed by concluding remarks.

## II. OPERATING PRINCIPLE OF CHM

The conceptual diagram of the proposed CHM is shown in Fig. 1. The CHM utilizes a pair of group coils (shown in Fig. 2a) which consist of three different coils. The square-shaped coils ( $L_{11}$  and  $L_{21}$ ) are resonating at the fundamental frequency and operate as a main power link. The other two pairs of 8-shaped coils,  $L_{21}$ - $L_{22}$  and  $L_{31}$ - $L_{33}$ , work as data links and resonate at 3<sup>rd</sup> and 7<sup>th</sup> harmonic frequencies, respectively (Fig. 2b). As shown in Fig. 3, the 8-shape coil is divided into two rectangular coils, and their magnetic fields are going in the opposite direction. Therefore, on the non-linked coils, the magnetic fluxes are canceling each, and their mutual inductances between non-linked coils become negligible. Therefore, the inductive links are independent of each other [14]

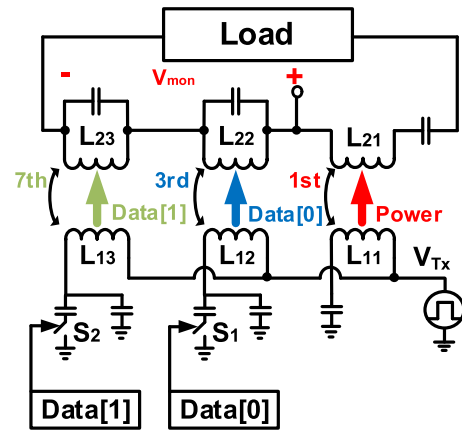


FIGURE 1. Conceptual diagram of CHM with the Tx/Rx group coils.

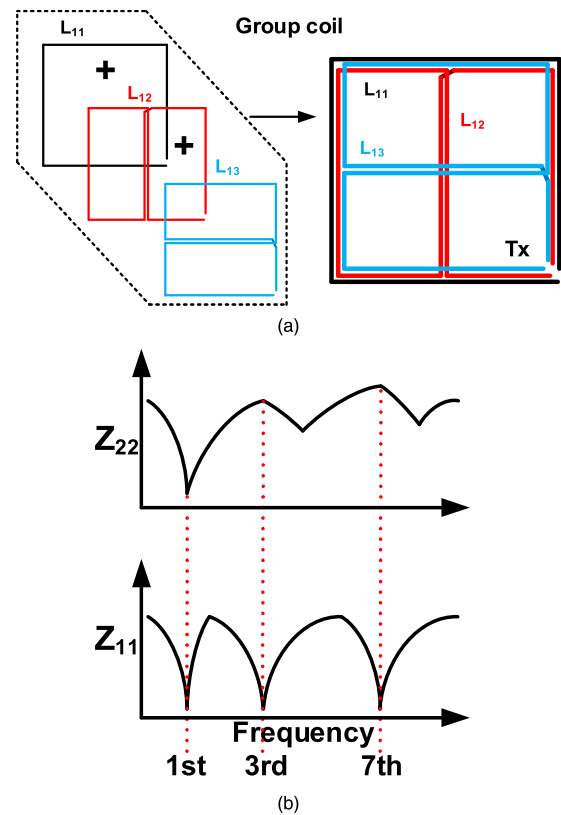


FIGURE 2. (a) Concept and (b) impedance of the group coil.

Based on Taylor series expansion, a square waveform can be approximated as

$$f(t) = \frac{4}{\pi} \left[ \sin(x) + \frac{\sin(3x)}{3} + \frac{\sin(5x)}{5} + \frac{\sin(7x)}{7} \dots \right]. \quad (1)$$

Accordingly, if we generate a square wave at the carrier frequency from a single class-D PA, it automatically generates odd harmonics without any frequency multiplier or additional oscillator. There was a study using the derived odd harmonics as an additional power source [12]. It improves PDL, but the

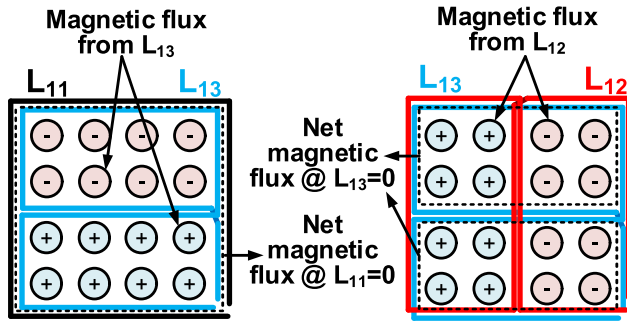


FIGURE 3. Direction of magnetic flux in the group coil.

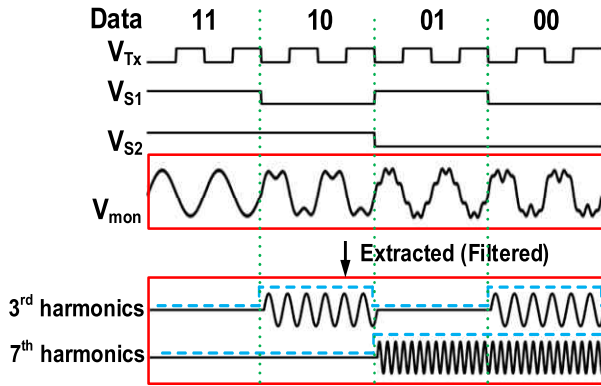


FIGURE 4. Conceptual waveform of the proposed CHM.

power transfer efficiency (PTE) was not improved because the harmonics are consuming extra power compared to the single coil WPT. We propose the CHM that can utilize the 3rd, 5th, and 7th harmonics as data links for transmitting 2-bit data simultaneously, instead of using power transmission. This is because the amplitude of these harmonics is about 1/3, 1/5, and 1/7 of the fundamental frequency, making them useful for transmitting data. In this paper, the 2-bit data transmission using 3rd and 7th harmonic LC-tanks is demonstrated considering the output impedance of the PA and data bandwidth. As the data rate increases, the widened 3rd harmonic spectrum band overlaps with the data band of the 5th harmonic, leading to an increase in Bit Error Rate (BER) caused by interference.

To utilize the harmonics, the group coil consists of three coils which are driven by a single common driver. To improve the power transfer efficiency (PTE), a multi-turn square-shaped coil that has a high Q is designed as a fundamental frequency link. To prevent interference from other links, we take advantage of orthogonal 8-shaped coils as 3rd and 7th harmonic data coils. Since the harmonic coils are utilized as the 2-bit data communication, we designed the 8-shaped coil as a single-turn coil which has a relatively low Q and wider bandwidth. In addition, as shown in Fig. 3, 8-shaped coils are orthogonally placed to diminish the magnetic interferences between them.

The conceptual waveform of the proposed CHM is shown in Fig. 4. A square wave is applied to the TX coils, and, depending on 2-bit digital data, Data[0] ( $= V_{S1}$ ) and Data[1]

( $= V_{S2}$ ), the fundamental and odd harmonics can be delivered to the RX coil. The switch has an internal ON-resistance that affects the Q-factor of the LC-tank when it is fully resonated at the power carrier frequency. To address this issue, we have set up the system such that when a switch is opened, the LC tank is resonating. As depicted in Fig. 4, if Data[n] is 1, a harmonic component will not be transmitted. Depending on the 2-bit data, the voltage difference between  $L_{22}$  and  $L_{23}$ ,  $V_{mon}$ , is modulated, and we can extract the data by checking the presence of harmonics on  $V_{mon}$ .

The summation of the coupled current on  $L_{21}$ ,  $L_{22}$ , and  $L_{23}$  is rectified and powered the load as a DC power source. The received 2-bit data stream is recovered by the envelope of 3rd and 7th frequency components from  $V_{mon}$ . Because the two data switches at the TX are independently controlled in the proposed CHM, 2-bit forward data can be delivered at the same time; one from the 3rd harmonic link and the other from the 7th harmonic link. The first bit is applied to the gate of  $S_1$  (Data[0] in Fig. 1) and the second bit is applied to the gate of  $S_2$  (data [1] in Fig. 2a). As mentioned above, harmonics are transmitted when a switch is opened, the envelope of harmonics is the inversion of the Data[n].

The schematic of the TX board is shown in Fig. 5a. The three LC-tanks are connected in parallel, and each coil has a series capacitor to resonate at the 1st, 3rd, and 7th frequencies, respectively. Except for the fundamental coil ( $L_{11}$ ) which delivers the power, other coils have a pair of detuning capacitors controlled by the switches. When either  $S_1$  or  $S_2$  is opened, the 3rd ( $L_{12}$ - $L_{22}$ ) or 7th ( $L_{13}$ - $L_{23}$ ) harmonic coil is resonating at the 3rd or 7th frequency while it is lower than the target frequency when the switches are closed. Since the detuning capacitor changes the equivalent reactance of the LC-tank, to prevent the capacitor affects the other LC resonance, we use a relatively small amount of capacitance compared to the resonating capacitor. The detuning about 20 dB lower than the resonating condition. As detuning capacitor switches ( $S_1$  and  $S_2$ ), back-to-back capacitance is determined to make the harmonics component NMOSs are used to completely float the capacitor in both positive and negative voltage applied on the LC-tank.

In Fig. 5b, the RX circuit has LCs that are in parallel resonance at harmonic frequencies. This configuration has two benefits: it maximizes  $V_{mon}$  and reduces impedance at the fundamental frequency. The fundamental frequency coil, on the other hand, is resonating in series, which is advantageous for small load resistances. To compensate for the small inductance contributed by the harmonic LCs, we chose a resonating capacitance that cancels out that inductance. To monitor the amplitude of harmonics, we need to monitor the induced current on the  $L_{22}$  and  $L_{23}$ . Instead of direct monitoring of the current, we monitor the voltage across the LC-tanks of  $L_{22}$  and  $L_{23}$  ( $V_{mon}$ ) which is proportional to the  $I_{L22}$  and  $I_{L23}$ . To maximize the voltage at the target frequency, parallel resonance that provides high impedance at the resonance was used on both LC-tanks of  $L_{22}$  and  $L_{23}$ . The parallel resonance is also beneficial for power transmission because

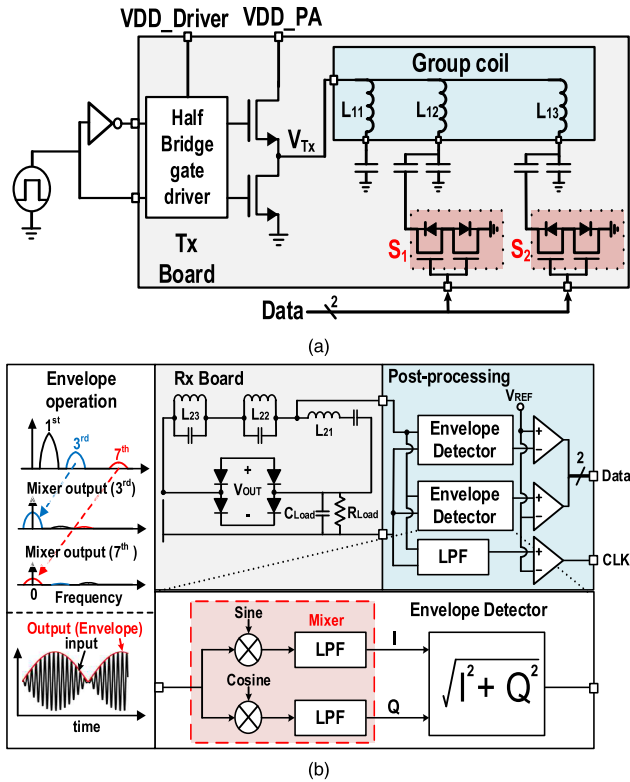


FIGURE 5. Circuit configurations of the (a) Tx and (b) Rx boards.

the equivalent impedance of the overall  $LC$ -tank composed of  $L_{22}$  and  $L_{23}$  becomes low at the fundamental frequency that is off-target. We used a lowpass filter (LPF) and an envelope detector to measure the power of the harmonics. As an envelope detector, we employ a direct down-conversion mixer that produces in-phase (I) and quadrature-phase (Q), and root-mean-square (RMS) of both outputs indicates the envelope of the signal. If the amount of harmonic power is larger than the threshold level, harmonics are in resonance ( $\text{Data}[n]$  is 0) and vice versa.

### III. IMPLEMENTATION AND MEASUREMENT RESULTS

The proof-of-the-concept board is populated with commercial off-the-shelf (COTS) (Fig. 6). As a class-D PA, we adopted ISL2110 (Renesas, Tokyo, Japan) as a gate driver and IRF530 (Infineon, Muenchen, Germany) as a power MOSFET. In the TX board, a back-to-back N-channel MOSFET (BSP89, Infineon, Muenchen, Germany) is implemented as a switch, which is controlled by the data bit stream. We designed a 5-turn square-shaped coil as the fundamental frequency link, and two single-turn 8-shaped coils were orthogonally wound inside of the square-shaped coil (Fig. 6) and used as the 3<sup>rd</sup> and 7<sup>th</sup> harmonic coils. The detailed specifications of coils are summarized in Table 1. As expected, the coupling coefficients between non-linked coils are negligible because the magnetic flux cancellation shown in Fig. 3 is properly worked.

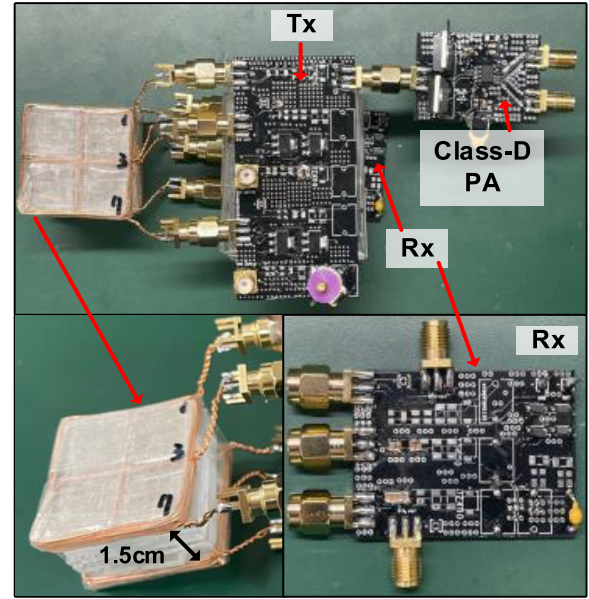


FIGURE 6. Measurement setup.

TABLE 1. Specifications of coils.

$L_{11}, L_{21}$	Number of turns	5
	Diameter (mm)	30
	Thickness (mm)	2.5
	$L$ ( $\mu\text{H}$ )	1.82
	$R$ ( $\Omega$ )	0.3
$L_{12}, L_{13}, L_{22}, L_{23}$	Number of turns	1
	Diameter (mm)	30
	Thickness (mm)	0.5
	$L$ ( $\mu\text{H}$ )	0.165
	$R$ ( $\Omega$ )	0.13
Power link	$k_{11,21}$	0.15
Data link	$k_{12,22}$	0.14
	$k_{13,23}$	0.14
Inter data link	$k_{12,13}$	0.02
	$k_{22,23}$	0.02
Power-data link	$k_{11,13}$	0.02
	$k_{21,23}$	0.02
	$k_{11,12}$	0.02
	$k_{21,22}$	0.02

We verified the SWIPT functionality with the arbitrary waveform generator that creates the random digital bit stream at TX. We sent the random data stream with a 550-kbps data rate per 3<sup>rd</sup> and 7<sup>th</sup> link, respectively, which is corresponding to the total data rate of 1.1 Mbps. The data rate should be sub-harmonic of carrier frequency since we utilize the extracted clock from the power carrier for the data recovery at the RX.

The measured waveforms of the proposed system with a distance of 1.5 cm are shown in Fig. 7. Envelope signals of the harmonic frequencies are matched with the inputted individual data stream ( $\text{Data}[0]$ ,  $\text{Data}[1]$ ). The envelope signals from the 3<sup>rd</sup> and 7<sup>th</sup> coils are compared with the reference voltage at the frequency of the recovered clock (CLK), and the results are recorded as 2-bit data stream. The measured

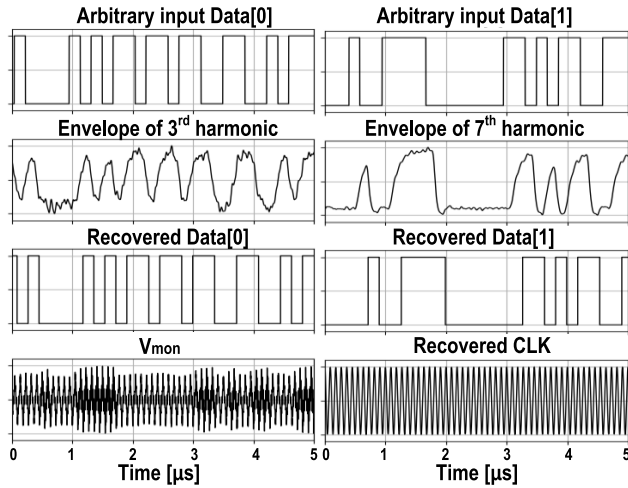


FIGURE 7. Measured transient waveforms with arbitrary input data (Data[0],Data[1]).

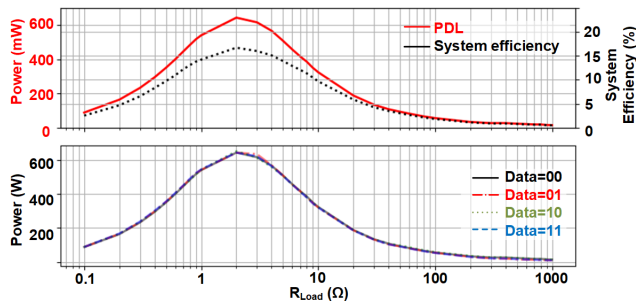


FIGURE 8. Measured system efficiency and PDL.

bit error rate (BER) is less than  $2.5 \times 10^{-5}$  while the load on RX simultaneously received the power of 641 mW.

The measured PDL and system efficiency are shown in Fig. 8. The system efficiency is measured from the power supply of the PA in TX to the rectifier output in RX (DC-to-DC). The maximum PDL is 641 mW and system efficiency is 17 % when the load is  $2 \Omega$ . The PTE of the coils shows 51% because the coil used in the analysis was not optimized at the operating frequency and the quality factor of it was measured as 42. The measured PDL is rarely changed by the data stream (Data[0] and Data[1]); the PDL changed less than 5% when load resistance ( $R_{Load}$ ) is less than  $100 \Omega$ . The  $L_{21}$  and the paired resonating capacitor are connected in series to provide better impedance matching at low  $R_{Load}$ , and the case where  $R_{Load}$  is larger than  $100 \Omega$  is out of focus in this prototype. To compare the PDL with different modulation techniques, we simulated ASK, PSK, FSK, and CHM under the same WPT condition. The proposed CHM shows the highest PDL with highest data rate (1.1 MHz) while ASK(modulation index = 10%), PSK and FSK (1MHz, 1.2MHz) only show the 86%, 11.5%, and 31% of PDL even at 110 kbps data rate.

Fig. 9 illustrates the effects of coil misalignment in a CHM system. Similar to conventional WPT technologies, the PTE in CHM systems decreases as the mutual inductance value,

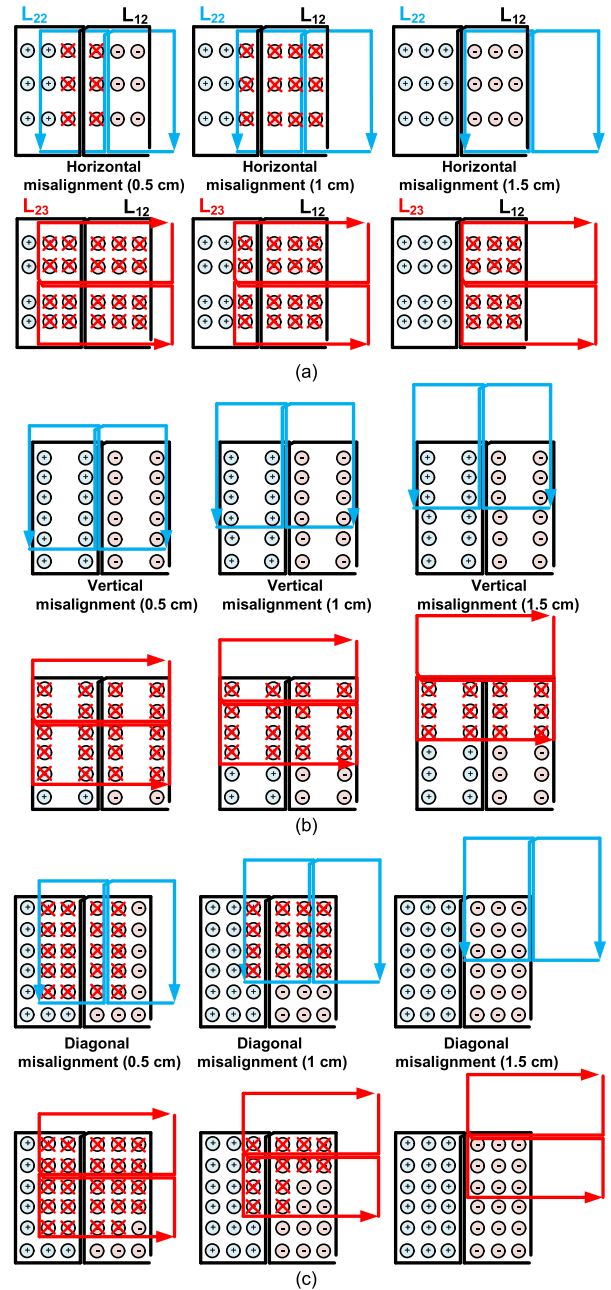


FIGURE 9. Effect of misalignment on magnetic flux in (a) horizontal, (b) vertical, and (c) diagonal directions.

which is proportional to the overlapped area of the coils, decreases. However, as shown in Fig. 8b, the BER does not monotonically decrease with coil misalignment. As depicted in Fig. 8c, 8-shaped coils used for harmonic (3<sup>rd</sup> or 7<sup>th</sup>) data transmission have a characteristic where magnetic flux is generated in different directions (up and down).

When the 8-shaped coils for Tx and Rx are horizontally displaced from the origin (as shown in Fig. 9a), the interconnected bidirectional flux produced by the Tx coil (upper part of Fig. 9a) counteracts itself within the Rx 8-shaped coil. This outcome diminishes the effective flux conveyed to the Rx

**TABLE 2.** Simultaneous wireless information and power transfer.

	[8]	[9]	[13]	[15]	[16]	[17]	This work
Power Carrier Frequency (MHz)	-	13.56	0.1	2/4	10	0.02	<b>1.1</b>
Data Carrier Frequency (MHz)	66.6	50	3.2	-	-	-	<b>-</b>
Distance (mm)	10	10	30	10	6	25	<b>15</b>
Coil Diameter (TX/RX, cm)		3.2/3.0	400/400	3.5/2	3/2	30/20	<b>3/3</b>
Modulation	PHM	PDM	ASK	FSK	ASK	FSK	<b>CHM</b>
Data Rate (Mbps)	20	13.56	0.6	0.8	0.1	0.00012	<b>1.1</b>
PDL (mW)	-	42	504000	140	10	700000	<b>641</b>
System efficiency (DC-to-DC)	-	-	83.3 %*	14 %	-	85 %*	<b>17 %</b>
Bit Error Rate(BER)	$8.7 \times 10^{-8}$	$4.3 \times 10^{-7}$	-	$< 10^{-5}$	-	-	<b><math>&lt; 2.5 \times 10^{-5}</math></b>
Data Rate / Power Carrier Frequency	0.3**	1	0.188	0.2	0.01	0.05	<b>1</b>
Additional data Driver	Yes	Yes	Yes	No	No	No	<b>No</b>

\*Power transfer efficiency (PTE)

\*\*Data Rate/ Data Carrier Frequency

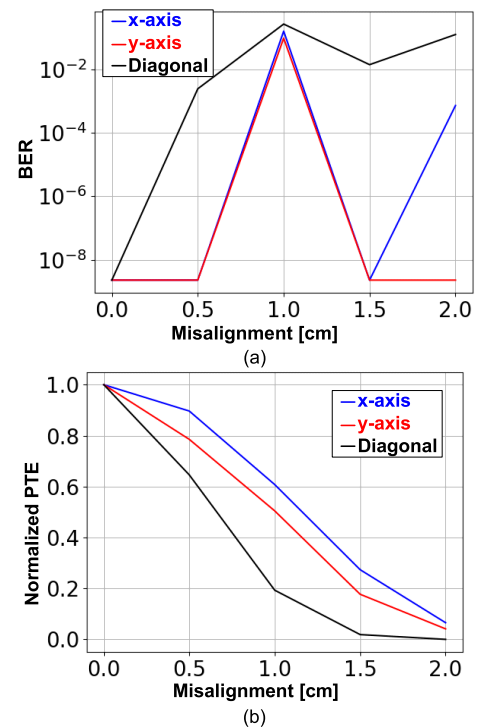
coil, resulting in suboptimal flux transfer. In particular, when Tx and Rx coils are misaligned horizontally by 1/3 of the coil size (1 cm in our work), all harmonic fluxes are canceled out in the Rx 8-shaped coil, leading to the worst BER.

Conversely, the magnetic flux generated by the different harmonic coils (ex. 3<sup>rd</sup> Tx coil to 7<sup>th</sup> Rx coil or 7<sup>th</sup> Tx coil to 3<sup>rd</sup> Rx coil) undergoes a complete cancellation, leading to an absence of energy transmission as shown in lower part of Fig. 9a. Consequently, this lack of energy transfer through different harmonic coils does not have a detrimental impact on BER.

In the case of vertical coil misalignment of 8-shaped coils (Fig. 9b), through the same harmonic coils (ex. 3<sup>rd</sup> Tx coil to 3<sup>rd</sup> Rx coil or 7<sup>th</sup> Tx coil to 7<sup>th</sup> Rx coil) as shown in upper part of Fig. 9b although the amount of received magnetic flux decreases due to the reduced overlapped area, the direction of the magnetic flux passing through the Rx 8-shaped coil does not change, so it does not cause serious problems with the BER. Considering the same harmonic coil scenario, the magnetic flux is subject to complete annulment. Analogous to the circumstances of horizontal misalignment, this cancellation of magnetic flux does not elevate BER.

Since the two harmonic coils (3<sup>rd</sup> and 7<sup>th</sup> coils) are orthogonally placed, if one harmonic coil moves vertically, the other moves horizontally. Therefore, movement in either the x or y direction will increase BER of one of the harmonics. As a result, both x and y direction movements exhibit similar patterns in BER.

In the case of diagonal misalignment, as depicted in Fig. 9c, the same harmonic coils (upper part of Fig. 9c) experienced a reduction in magnetic flux intensity due to the phenomenon of cancellation. Furthermore, the magnetic flux transmitted from the different harmonic coils (lower part of Fig. 9c) does not achieve complete cancellation. Consequently, these different harmonic coils introduce extraneous noise to Rx coil. This effect is observed in both the 3<sup>rd</sup> and 7<sup>th</sup> harmonics, resulting in an increment of BER when compared to situations in orthogonal misalignments (Fig. 10). As depicted

**FIGURE 10.** Effect of misalignment on (a) BER and (b) PTE.

in Fig. 11, the system efficiency decreases as the distance between coils increases, concurrently leading to an elevation in BER due to the weakening link between both power and data coils.

Table 2 summarizes the comparison among the prior works. A data rate of a typical SWIPT system is less than the power carrier frequency because the data is modulated and transferred through the power carrier. To achieve the higher data rate, either a higher power carrier frequency or a separate data driver for additional data link, designed with a higher data carrier frequency than the power carrier frequency, is necessary [9]. However, the proposed CHM

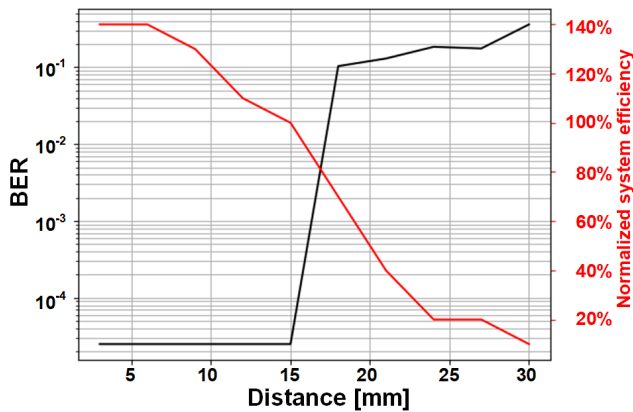


**FIGURE 11.** Normalized system efficiency and BER with distance (normalized at 15 mm).

achieved a higher data rate within the low power carrier frequency resulting in the best data rate per carrier frequency without the additional data driver on the TX. Other prior works which do not use the separate data driver only achieved less than 0.2 of data rate/carrier frequency.

#### IV. CONCLUSION

We have presented a new concept of CHM which transmits both wireless data and power without the additional data driver maintaining the high PDL. The CHM utilizes the group coil which consists of three coils on the same plane and diameter. The proposed CHM shows less than 5% PDL variation with the simultaneous 2-bit data transmission. It shows a maximum PDL of 641 mW and overall system efficiency of 17%. The measured data rate is 1.1 Mbps with a BER of  $< 2.5 \times 10^{-5}$ .

#### REFERENCES

- [1] T. D. P. Perera, D. N. K. Jayakody, S. K. Sharma, S. Chatzinotas, and J. Li, "Simultaneous wireless information and power transfer (SWIPT): Recent advances and future challenges," *IEEE Commun. Surveys Tuts.*, vol. 20, no. 1, pp. 264–302, 1st Quart., 2018.
- [2] K. W. Choi, S. I. Hwang, A. A. Aziz, H. H. Jang, J. S. Kim, D. S. Kang, and D. I. Kim, "Simultaneous wireless information and power transfer (SWIPT) for Internet of Things: Novel receiver design and experimental validation," *IEEE Internet Things J.*, vol. 7, no. 4, pp. 2996–3012, Apr. 2020, doi: 10.1109/JIOT.2020.2964302.
- [3] J. Wu, C. Zhao, Z. Lin, J. Du, Y. Hu, and X. He, "Wireless power and data transfer via a common inductive link using frequency division multiplexing," *IEEE Trans. Ind. Electron.*, vol. 62, no. 12, pp. 7810–7820, Dec. 2015.
- [4] J. Besnoff, M. Abbasi, and D. S. Ricketts, "High data-rate communication in near-field RFID and wireless power using higher order modulation," *IEEE Trans. Microw. Theory Techn.*, vol. 64, no. 2, pp. 401–413, Feb. 2016.
- [5] J. Wu, C. Zhao, Z. Lin, J. Du, Y. Hu, and X. He, "Wireless power and data transfer via a common inductive link using frequency division multiplexing," *IEEE Trans. Ind. Electron.*, vol. 62, no. 12, pp. 7810–7820, Dec. 2015.
- [6] J.-G. Kim, G. Wei, M.-H. Kim, H.-S. Ryo, and C. Zhu, "A wireless power and information simultaneous transfer technology based on 2FSK modulation using the dual bands of series-parallel combined resonant circuit," *IEEE Trans. Power Electron.*, vol. 34, no. 3, pp. 2956–2965, Mar. 2019.
- [7] A. N. Laskovski and M. R. Yuce, "Multi-node body area networks using harmonics-based telemetry implants," in *Proc. 4th Int. Symp. Appl. Sci. Biomed. Commun. Technol. (ISABEL)*, Oct. 2011, pp. 151:1–151:5.
- [8] M. Kiani and M. Ghovanloo, "A 20-Mb/s pulse harmonic modulation transceiver for wideband near-field data transmission," *IEEE Trans. Circuits Syst. II, Exp. Briefs*, vol. 60, no. 7, pp. 382–386, Jul. 2013, doi: 10.1109/TCSII.2013.2261182.
- [9] M. Kiani and M. Ghovanloo, "A 13.56-Mbps pulse delay modulation based transceiver for simultaneous near-field data and power transmission," *IEEE Trans. Biomed. Circuits Syst.*, vol. 9, no. 1, pp. 1–11, Feb. 2015.
- [10] B. Lee and M. Ghovanloo, "An overview of data telemetry in inductively powered implantable biomedical devices," *IEEE Commun. Mag.*, vol. 57, no. 2, pp. 74–80, Feb. 2019.
- [11] Z. Yan, C. Ma, Z. Zhang, L. Huang, and P. A. Hu, "Redefining the channel bandwidth for simultaneous wireless power and information transfer," *IEEE Trans. Ind. Electron.*, vol. 69, no. 7, pp. 6881–6891, Jul. 2022.
- [12] H. Zhang, Y.-X. Guo, S.-P. Gao, and W. Wu, "Wireless power transfer antenna alignment using third harmonic," *IEEE Microw. Wireless Compon. Lett.*, vol. 28, no. 6, pp. 536–538, Jun. 2018.
- [13] P. Wang, Y. Sun, Y. Feng, T. Feng, Y. Fan, and X. Li, "An improvement of SNR for simultaneous wireless power and data transfer system with full-duplex communication mode," *IEEE Trans. Power Electron.*, vol. 37, no. 2, pp. 2413–2424, Feb. 2022, doi: 10.1109/TPEL.2021.3106903.
- [14] I. Ghotbi, M. Najjarzadegan, H. Sarfaraz, S. Jafarabadi Ashtiani, and O. Shoaie, "Enhanced power-delivered-to-load through planar multiple-harmonic wireless power transmission," *IEEE Trans. Circuits Syst. II, Exp. Briefs*, vol. 65, no. 9, pp. 1219–1223, Sep. 2018.
- [15] H. Jung and B. Lee, "Wireless power and bidirectional data transfer system for IoT and mobile devices," *IEEE Trans. Ind. Electron.*, vol. 69, no. 11, pp. 11832–11836, Nov. 2022.
- [16] Y.-P. Lin, C.-Y. Yeh, P.-Y. Huang, Z.-Y. Wang, H.-H. Cheng, Y.-T. Li, C.-F. Chuang, P.-C. Huang, K.-T. Tang, H.-P. Ma, Y.-C. Chang, S.-R. Yeh, and H. Chen, "A battery-less, implantable neuro-electronic interface for studying the mechanisms of deep brain stimulation in rat models," *IEEE Trans. Biomed. Circuits Syst.*, vol. 10, no. 1, pp. 98–112, Feb. 2016.
- [17] C.-C. Huang and C.-L. Lin, "Wireless power and bidirectional data transfer scheme for battery charger," *IEEE Trans. Power Electron.*, vol. 33, no. 6, pp. 4679–4689, Jun. 2018.



**JAEMYUNG LIM** (Member, IEEE) received the bachelor's degree in electrical and computer engineering from Hanyang University, Seoul, South Korea, and the M.S. and Ph.D. degrees in electrical and computer engineering from Georgia Tech, Atlanta, GA, USA.

He was with Apple Inc., as a Custom Circuit Designer of application processors, from 2017 to 2022. He is currently an Assistant Professor with the Department of Electronic Engineering, Hanyang University. His research interests include power management IC, power architecture design, ultrasound related systems, and display driver IC.



**BYUNGHUN LEE** (Member, IEEE) received the B.S. degree from Korea University, Seoul, South Korea, in 2008, the M.S. degree from the Korea Advanced Institute of Technology (KAIST), Daejeon, South Korea, in 2010, and the Ph.D. degree in electrical and computer engineering from the Georgia Institute of Technology (Georgia Tech), in 2017. From 2010 to 2011, he was involved on wireless power transfer systems for electric vehicles with KAIST, as a Research Engineer. From 2017 to 2021, he was with the Department of Electrical Engineering, Incheon National University, Incheon, South Korea, as an Assistant Professor. He is currently an Assistant Professor with the Department of Biomedical/Electronic Engineering, Hanyang University, and the Director of the BCAS Laboratory. He served as the General Chair for the IEEE Wireless Power Week (WPW) 2020, South Korea.

...